Hindawi
International Journal of Aerospace Engineering
Volume 2024, Article ID 2054883, 14 pages
https://doi.org/10.1155/2024/2054883

Research Article

Fault-Tolerant Control for Carrier-Based Aircraft Automatic Landing Subject to Multiple Disturbances and Actuator Faults

Qilong Wu and Qidan Zhu

College of Intelligent Systems Science and Engineering, Harbin Engineering University, Harbin, Heilongjiang 150001, China

Correspondence should be addressed to Qidan Zhu; zhuqidan@hrbeu.edu.cn

Received 21 August 2023; Revised 26 February 2024; Accepted 8 March 2024; Published 26 March 2024

Academic Editor: Chen Pengyun

This paper introduces a fault-tolerant control scheme for the automatic carrier landing of carrier-based aircraft using direct lift control. The scheme combines radial basis function neural network and active disturbance rejection control (RBF-ADRC) to overcome the impact of actuator failures and external disturbances. First, the carrier-based aircraft model, the carrier air-wake model, and the actuator fault model were established. Secondly, ADRC is designed to estimate and compensate for actuator faults and disturbances in real time. RBFNN adjusts the ADRC controller parameters based on the system state. Then, the Lyapunov function is constructed to prove the stability of the closed-loop system. The controller is applied to the direct lift control channel, auxiliary attitude channel, and approach power compensation system. The direct lift control improves the performance of fixed-wing aircraft. Finally, comparative simulations were conducted under various actuator failures. The results demonstrate the remarkable fault tolerance of the RBF-ADRC scheme, enabling precise tracking of the desired glide path by the shipboard aircraft even in the presence of actuator failures.

1. Introduction

Carrier-based aircraft landing technology has received extensive attention as a prerequisite for effective combat applications at sea [1, 2]. The automatic carrier landing system (ACLS) comprises the aircraft flight control system, approach power compensator system, inertial navigation sensors, and precision tracking radar, enabling automated approach control to the carrier deck in all weather conditions. Various intelligent control methods, such as adaptive sliding mode control [3], backstepping and sliding mode [4], adaptive preview control [5], fixed-time backstepping control [6], and inverse optimal control [7], are employed in the ACLS to track the desired glide path during the landing process precisely. Furthermore, the ACLS incorporates adaptive backstepping sliding mode control to mitigate the impact of carrier air-wake turbulence during the landing process [8]. The above studies focus on the conventional maneuvering of shipboard aircraft under ideal conditions without any faults. The conventional aircraft maneuvering method involves utilizing the elevator to alter the pitch attitude of the aircraft and subsequently modify its flight trajectory. However, this approach has inherent limitations, including trajectory-attitude coupling and insufficient landing accuracy. Consequently, the direct lift control is proposed for the automatic carrier landing system (DLC-ACLS) [9, 10]. This technology directly manipulates the force exerted on the aircraft through the flap, eliminating the coupling between trajectory and attitude. Nevertheless, potential actuator failures and other factors during the automatic landing of the shipboard aircraft can considerably impact the landing accuracy, even when utilizing DLC. Hence, it is imperative to incorporate controller fault tolerance performance in the design of DLC-ACLS.

For the design of fault-tolerant control systems for aircraft, many experts have designed different schemes [11–13]. Model

predictive control is more widely used in fault-tolerant control, and the literature [14] proposed a fault-tolerant controller using nonlinear model predictive control (NMPC) that can effectively recover a damaged quadrotor. However, MPC requires accurate system models to calculate the control signal. Moreover, failures can lead to sudden changes in model parameters that cannot be predicted in advance. Sliding mode control and backstepping techniques applied to an aircraft fault-tolerant control system allow the dynamic stability of the aircraft to converge [15, 16], but the computational complexity is notably high. The literature [17] uses adaptive controllers that can automatically update parameters to compensate for actuator failures in the system, but adaptive control exhibits limited adaptability to swift system changes, particularly when encountering significant model alterations. A fault-tolerant scheme known as antiwindup incremental nonlinear dynamic inversion (INDI) is proposed for flying wing aircraft afflicted with actuator faults [18]. Nonetheless, the NDI control method heavily relies on the accuracy of the model, and the control performance of the dynamic inverse controller will drop sharply when the model data is imprecise. Consequently, active disturbance rejection control (ADRC) has garnered growing attention. Literature [19, 20] optimizes the controller parameters using an optimization algorithm. Waves cause irregular movements of the deck, making the landing process difficult [21]. Literature [22] improves the accuracy of the landing phase by introducing an algorithm for predicting the motion of the deck of the carrier-based aircraft in the automatic landing system.

The ADRC method, a novel model-independent nonlinear controller, enjoys significant popularity in practical engineering applications. It has been successfully applied in many fields due to its simplicity, strong robustness, and immunity to disturbances. In literature [23], the UAV attitude control is designed, and the perturbations and uncertainties can be well estimated and eliminated online using the ADRC and embedded model control methods. The decoupled design of a fighter's three channels utilizing ADRC treats the coupling between different channels as a comprehensive perturbation, effectively estimating and compensating for this disturbance [24]. For fractional-order systems with uncertainty, a combined fractional tracking controller that integrates backstepping and ADRC is introduced [25].

Although ADRC has the above advantages, when the carrier-based aircraft is affected by external disturbances and ESO estimation errors, a set of fixed feedback rate parameters makes the control efficiency unsatisfactory. RBF neural network can effectively control complex uncertain systems due to its ability of learning and self-adaptation [26–28]. In order to simplify the parameter adjustment process and enhance the fault-tolerant control capability of the controller, the automatic landing control system can quickly and stably fly along the ideal glide path under the conditions of actuator failure and external disturbance. This paper presents a new method for online automatic tuning of ADRC parameters using RBFNN. And the strategy is applied to the control of DLC-ACLS. The stability of the control system is analyzed using the Lyapunov stability theory, and the simulation results are compared with ADRC and PID. Compared with the literature [29], the model in this paper is more accurate and the control method is more practical. The results show that the method can quickly and stably track the ideal glide slope and has good robustness to external disturbances. The main contributions of this work are shown as follows:

(1) A novel fault-tolerant control technique based on the combination of RBFNN and ADRC is designed. The proposed control scheme handles actuator failures, internal uncertainties, and external disturbances in real time, enhancing the system's robustness. The ESO accurately observed and suppressed the disturbance through the state feedback controller, significantly improving the success rate of carrier-based aircraft landing. This control method compensates for actuator failures and airwake disturbances that seriously affect landing accuracy and safety

(2) The automatic control system consisting of a flight trajectory control system, attitude control system, and APCS is designed. The stability of the closed-loop system after introducing the RBF neural network is proved by constructing the Lyapunov function

The structure of this paper is as follows: in Section 2, the nonlinear model of carrier-based aircraft, the carrier airwake model, and the actuator fault model are described. The control method of RBFNN to adjust the ADRC parameters is designed in Section 3, and the control method is applied to the DLC-ACLS in Section 4; in Section 5, simulation results are used to demonstrate the effectiveness of the proposed control method; the conclusion is presented in Section 6.

2. Landing Model Building

The final landing phase is shown in Figure 1. This section describes the aircraft nonlinear model, the carrier air-wake model, and the actuator failure model. According to the literature [30], the control inputs include elevator rudder (δ_e), trailing edge flaps (δ_f) and thrust (P), as shown in Figure 2.

2.1. Nonlinear Modeling of Carrier-Based Aircraft. This section gives the kinematic and dynamical model of the carrier-based aircraft. Define the coordinate system: the geodetic coordinate system (inertial coordinate system) $O_g x_g y_g z_g$ is denoted as S_g with the earth fixed, and any point on the surface is chosen as the origin. The trajectory coordinate system $Ox_k y_k z_k$ is denoted as S_k, the airframe coordinate system $Ox_b y_b z_b$ is denoted as S_b with the aircraft fixed, and the center of mass is generally chosen as the origin. The airflow coordinate system $Ox_a y_a z_a$ is

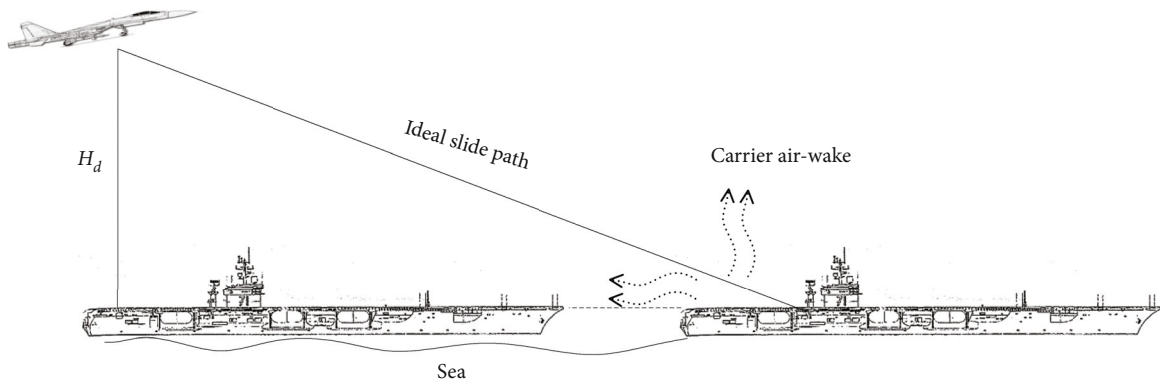

Figure 1: Final carrier landing phase.

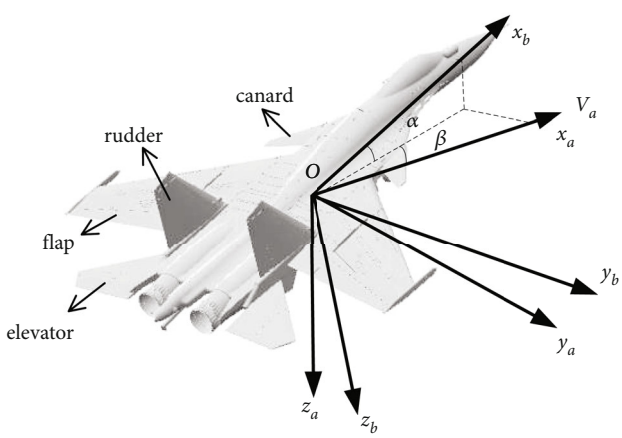

Figure 2: Control surfaces of the target aircraft.

denoted as S_a, and O_b represents the geometric center of the aircraft.

$$\begin{cases} \dot{V} = \dfrac{1}{m}(P\cos\alpha\cos\beta - D - mg\sin\gamma), \\ \dot{\chi} = \dfrac{1}{mV\cos\gamma}[P(\sin\alpha\sin\mu - \cos\alpha\sin\beta\cos\mu) + C\cos\mu + Y\sin\mu], \\ \dot{\gamma} = \dfrac{1}{-mV}(P(-\sin\alpha\cos\mu - \cos\alpha\sin\beta\sin\mu) + C\sin\mu - Y\cos\mu + mg\cos\gamma, \end{cases}$$
$$\begin{cases} \dot{\alpha} = q - (p\cos\alpha + r\sin\alpha)\tan\beta - \dot{\gamma}\dfrac{\cos\mu}{\cos\beta} - \dot{\chi}\dfrac{\sin\mu\cos\gamma}{\cos\beta}, \\ \dot{\beta} = p\sin\alpha - r\cos\alpha - \dot{\gamma}\sin\mu + \dot{\chi}\cos\mu\cos\gamma, \\ \dot{\mu} = p\dfrac{\cos\alpha}{\cos\beta} + r\dfrac{\sin\alpha}{\cos\beta} + \dot{\gamma}\tan\beta\cos\mu + \dot{\chi}(\sin\gamma + \tan\beta\sin\mu\cos\gamma), \end{cases}$$
$$\begin{cases} \dfrac{dp}{dt} = \dfrac{1}{I_zI_x - I_{zx}^2}\left[I_zL_r + I_{zx}N - I_{zx}(I_y - I_x - I_z)pq - (I_z^2 - I_zI_y + I_x^2)qr\right], \\ \dfrac{dq}{dt} = \dfrac{M + I_x(r^2 - p^2) + (I_z - I_x)pr}{I_y}, \\ \dfrac{dr}{dt} = \dfrac{1}{I_zI_x - I_{zx}^2}\left[I_{xx}L_r + I_xN + I_{zx}(I_y - I_x - I_z)qr + (I_x^2 - I_xI_y + I_{zx}^2)pq\right], \end{cases} \tag{1}$$

where V is the ground speed; γ is the flight trajectory angle; χ is the heading angle; α, β, and μ denote the angle of attack, sliding angle, and the roll angle; p, q, and r denote the angular rates; L_r, M, and N are roll moment, pitch moment, and yaw moment; P is the engine thrust; Y, D, and C are lift, drag, and lateral force; I_x, I_y, and I_z are the moments of inertia of the carrier aircraft; and I_{zx} is the product of inertia of the carrier aircraft.

2.2. Carrier Air-Wake Modeling. The carrier air-wake was modeled based on the US military standard MIL-F-8785C [31]. The air-wake consists of horizontal longitudinal component, horizontal lateral component, and vertical component. The corresponding equations are presented as follows:

$$\begin{cases} u = u_1 + u_2 + u_3 + u_4, \\ v = v_1 + v_4, \\ w = w_1 + w_2 + w_3 + w_4, \end{cases} \tag{2}$$

where u_1, v_1, and w_1 are free air turbulence components, u_2 and w_2 are steady components, u_3 and w_3 are periodic components, and u_4, v_4, and w_4 are random components, respectively.

2.3. Actuator Fault Model and Engine Dynamics. The typical actuator and engine dynamics are given as

$$\frac{\delta_Z}{\delta_{Z_c}} = \frac{\omega}{s + \omega}, \tag{3}$$

where the subscript c refers to the command.

Common actuator failures include jamming, drift, damage, and saturation. This paper focuses on the drift fault, and the fault model is as follows:

$$\delta = \delta_c + \rho, \tag{4}$$

where ρ represents the drift fault, which is divided into constant value fault and time-varying fault.

3. Controller Design

3.1. RBF Neural Network. RBF neural networks are 3-layer feedforward networks with a single hidden layer [32], as shown in Figure 3. RBF networks simulate the structure of

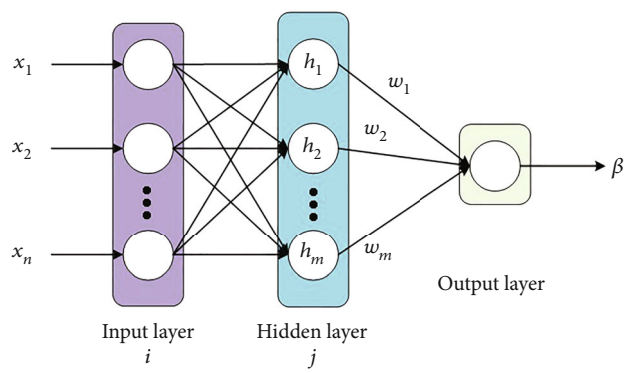

Figure 3: RBF neural network structure diagram.

locally tuned neural networks in the human brain, and it has been shown that RBF networks can approximate any continuous function with arbitrary accuracy [33].

The action function in the RBF network is a Gaussian function.

$$h_j = \exp\left(-\frac{\|X - C_j\|^2}{2b_j^2}\right), \tag{5}$$

where $X = [x_1, x_2, \cdots, x_n]^T$ is the input vector for the network; C_j is the center vector of node j, $C_j = [c_{j1}, c_{j2}, \cdots, c_{ji}, \cdots, c_{jn}]^T$, $j = 1, 2, \cdots, m$; b_j is the base width parameter of node j, $b_j > 0$.

Weight vector of the network is

$$W = [w_1, w_2, \cdots, w_j, \cdots, w_m]^T. \tag{6}$$

The output of the network is

$$\beta = w_1 h_1 + w_2 h_2 + \cdots + w_j h_j + \cdots + w_m h_m. \tag{7}$$

3.2. ADRC Optimized by RBF Neural Network. Take the example of a second-order system with faults

$$\ddot{x} = b(u + u_f) + f(x) = bu + \underbrace{bu_f + f(x)}_{f_0} = bu + f_0, \tag{8}$$

where $f_0 = bu_f + f(x)$ is the total disturbance of the system; equation (8) is written in the following form.

$$\begin{cases} \dot{x}_1 = x_2, \\ \dot{x}_2 = f_0 + bu, \\ y = x_1. \end{cases} \tag{9}$$

In order to make the output track the reference signal, it is necessary to design the second-order RBF-ADRC scheme. The controller will be constructed in detail below.

3.2.1. Tracking Differentiator (TD). The TD arranges the transition process for the input signal, and by selecting the appropriate parameters, it can prevent sudden changes in the input signal and improve the robustness of the control system [34]. The specific implementation of TD is shown in

$$\begin{cases} \dot{v}_1 = v_2, \\ \dot{v}_2 = \mathrm{fhan}(v_1 - x_d, v_2, r_0, r_1), \end{cases} \tag{10}$$

where x_d represents the desired instruction, r_0 is the velocity factor, r_1 is the filter factor, and fhan specific form reference literature [35].

3.2.2. ESO Design. The extended state observer (ESO) is a new type of disturbance observer, first proposed by Han [36]. The third-order ESO is designed according to equation (9). Using the idea of linearizing the dynamic compensation and treating the sum perturbation in the second-order system as an expanded state variable, equation (9) becomes as follows.

$$\begin{cases} \dot{x}_1 = x_2, \\ \dot{x}_2 = x_3 + bu, \\ \dot{x}_3 = \dot{f}_0. \end{cases} \tag{11}$$

To build a third-order ESO based on the above equation,

$$\begin{cases} e = z_1 - y, \\ \dot{z}_1 = z_2 - \beta_1 e, \\ \dot{z}_2 = z_3 - \beta_2 e + bu, \\ \dot{z}_3 = -\beta_3 e, \end{cases} \tag{12}$$

where z_1 is a highly accurate estimate of y, z_3 is an estimate of the overall perturbation, and $\beta_i (i = 1, 2, 3)$ is the observer gain. To ensure the estimation performance, the value of β_i can be set to [37]

$$\beta_i = \frac{(n+1)!}{i!(n+1-i)!} w_0^i (i = 1, 2, 3), \tag{13}$$

where w_0 is the observer bandwidth.

3.2.3. State Error Feedback (SEF). With ESO accurately estimating the total disturbance, the controller is given

$$u = \frac{u_0 - z_3}{b}. \tag{14}$$

Ignoring the estimation error of z_3 reduces the system to a unit gain cascade integrator system

$$\ddot{x} = (f - z_3) + u_0 \approx u_0. \tag{15}$$

The cascaded integrator system can be easily controlled by the following nonlinear state error feedback law.

$$\begin{cases} e_1 = v_1 - z_1, \\ e_2 = v_2 - z_2, \\ u_0 = \beta_1 fal(e_1, a_1, \delta) + \beta_2 fal(e_2, a_2, \delta), \\ u = u_0 - \dfrac{z_3}{b}. \end{cases} \tag{16}$$

In the above equation, the nonlinear function $fal(e, \varepsilon, \delta)$ is as follows:

$$fal(e, \varepsilon, \delta) = \begin{cases} \dfrac{e}{\delta^{(1-\varepsilon)}}, |e| \le \delta \\ \text{sign}\ (e)|e|^{\varepsilon}, |e| > \delta. \end{cases} \tag{17}$$

In order to simplify the parameter setting, RBFNN is introduced to adjust β_1 and β_2 in real time.

The performance index function of the RBFNN is

$$E(k) = \frac{1}{2} e(k)^2 = \frac{1}{2} (y(k) - y_c(k))^2. \tag{18}$$

According to the gradient descent method, the iterative algorithm of output weight vector, node center vector, and node base width parameters is

$$\begin{aligned} \Delta w_j(k) &= \eta(y(k) - y_c(k))h_j, \\ \Delta b_j(k) &= \eta(y(k) - y_c(k))\omega_j h_j \frac{\|X - C_j\|^2}{b_j^3}, \\ b_j(k) &= b_j(k-1) + \Delta b_j + \alpha\big(b_j(k-1) - b_j(k-2)\big), \\ \Delta c_{ji}(k) &= \eta(y(k) - y_c(k))\omega_j \frac{x_i - c_{ji}}{b_j^2}, \\ c_{ji}(k) &= c_{ji}(k-1) + \Delta c_{ji}(k) + \alpha\big(c_{ji}(k-1) - c_{ji}(k-2)\big), \end{aligned} \tag{19}$$

where η is for the learning rate and α is for the momentum factor.

3.3. Stability Analysis. This section analyzes the stability of the closed-loop system and derives the convergence time.

The Lyapunov function is constructed as follows.

$$V(k) = \frac{1}{2} (y(k) - y_c(k))^2 = \frac{1}{2} e^2(k). \tag{20}$$

According to equation (20), the change in the Lyapunov function is obtained by

$$\Delta V(k) = V(k+1) - V(k) = \frac{1}{2}\left[e^2(k+1) - e^2(k)\right]. \tag{21}$$

The weights are updated by the amount

$$\begin{aligned} \Delta w_j &= -\eta_w \frac{\partial E}{\partial w_j} = -\eta_w \frac{\partial E}{\partial y_c}\frac{\partial y_c}{\partial w_j} = \eta_w e h_j, \\ \Delta b_j &= -\eta_b \frac{\partial E}{\partial b_j} = -\eta_b \frac{\partial E}{\partial y_c}\frac{\partial y_c}{\partial b_j} = \eta_b e w_j h_j \frac{\|\mathbf{X} - \mathbf{C}_j\|^2}{b_j^3}, \\ \Delta c_j &= -\eta_c \frac{\partial E}{\partial c_j} = -\eta_b \frac{\partial E}{\partial y_c}\frac{\partial y_c}{\partial c_j} = \eta_c e w_j h_j \frac{x_i - c_{ji}}{b_j^2}. \end{aligned} \tag{22}$$

Since $\Gamma_x(k) = \partial y_c / \partial \mathbf{x}$, for $\mathbf{x} = w$, b, and c, it reveals that

$$\begin{aligned} \Gamma_w(k) &= \frac{\partial y_c}{\partial w} = \left[\frac{\partial y_c}{\partial w_1}, \cdots, \frac{\partial y_c}{\partial w_m}\right]^T, \\ \Gamma_b(k) &= \frac{\partial y_c}{\partial b} = \left[\frac{\partial y_c}{\partial b_1}, \cdots, \frac{\partial y_c}{\partial b_m}\right]^T, \\ \Gamma_c(k) &= \frac{\partial y_c}{\partial c} = \left[\frac{\partial y_c}{\partial c_1}, \cdots, \frac{\partial y_c}{\partial c_m}\right]^T, \end{aligned} \tag{23}$$

where

$$\begin{cases} \dfrac{\partial y_c}{\partial w_j} = h_j, \\ \dfrac{\partial y_c}{\partial b_j} = w_j h_j \dfrac{\|\mathbf{X} - \mathbf{C}_j\|^2}{b_j^3}, \\ \dfrac{\partial y_c}{\partial c_j} = w_j h_j \dfrac{x_i - c_{ji}}{b_j^2}. \end{cases} \tag{24}$$

The linearized model of the error equation can be represented as

$$e(k+1) = e(k) + \Delta e(k) \cong e(k) + \left[\frac{\partial e(k)}{\partial \mathbf{x}}\right]^T \mathbf{x}. \tag{25}$$

Using equation (18) yields

$$\frac{\partial e(k)}{\partial \mathbf{x}} = \frac{\partial e(k)}{\partial y_c}\frac{\partial y_c}{\partial \mathbf{x}} = -\Gamma_x(k). \tag{26}$$

Using equations (25) and (26) gives

$$e(k+1) = e(k) - [\Gamma_x(k)]^T \eta_x e \Gamma_X(k) = e(k)\left[1 - \eta_x \Gamma_x(k)^T \Gamma_x(k)\right]. \tag{27}$$

From equation (21) and (27), $\Delta V(k)$ can be represented as

$$\Delta V(k) = \frac{1}{2} e^2(k) \eta_x \|\Gamma_x(k)\|^2 \left[\eta_x \|\Gamma_x(k)\|^2 - 2\right]. \tag{28}$$

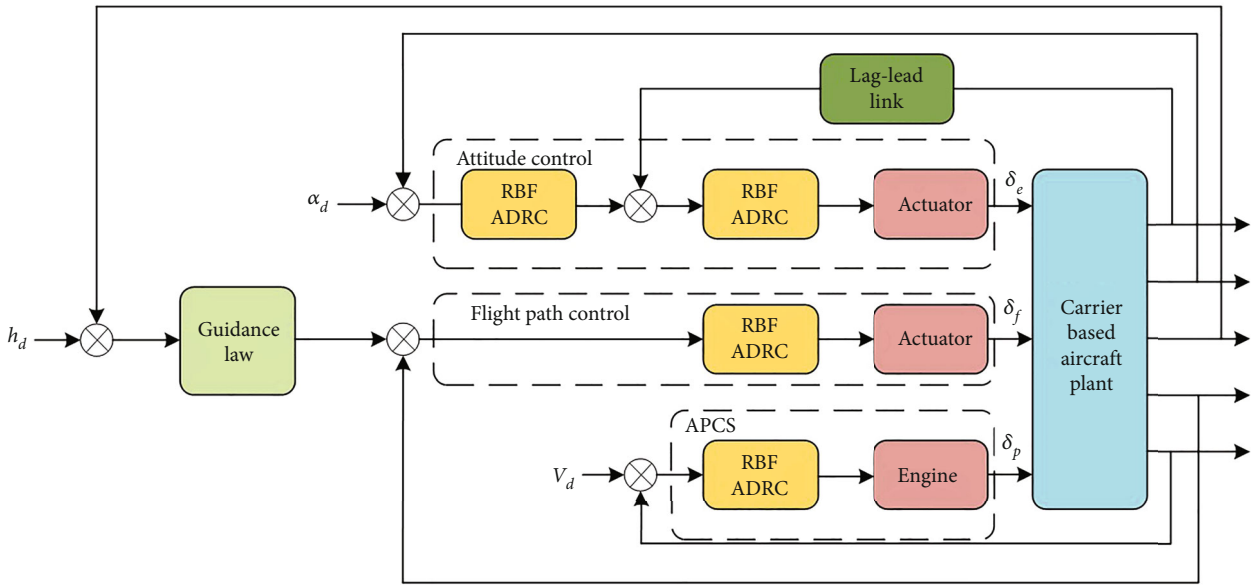

Figure 4: Diagram of the direct lift automatic landing system based on RBF-ADRC.

If η_x is chosen as

$$0 < \eta_x < \frac{2}{\|\Gamma_x(k)\|^2}, \tag{29}$$

then $\Delta V(k)$ in equation (29) will be less than zero. Therefore, the Lyapunov stability of $V > 0$ and $\dot{V} < 0$ is guaranteed.

4. Design of the Direct Lift Automatic Carrier Landing System Based on RBF-ADRC

The DLC-ACLS is shown in Figure 4. The main design of the system is based on three channels: the flight path control channel, the attitude control channel, and the APCS. The main flight path control channel receives the longitudinal guidance law command and generates the flap deflection command, the main purpose of which is to adjust the longitudinal altitude. The attitude control channel makes the attitude stable by adjusting the elevator, and the APCS keeps the speed stable by adjusting the throttle lever. The role of the longitudinal guidance law is to convert the altitude command into a trajectory angle command. The detailed design procedure will be explained in the following.

4.1. Attitude Channel Controller Design Scheme. The attitude control channel contains angular control and angular velocity control with the main purpose of maintaining the desired angle of attack, which is set to a constant value.

There is a strong coupling between the longitudinal and lateral motions of the aircraft, and in this case, the lateral coupling is treated as an additional perturbation by ADRC. We design the controller for the inner and outer loops of the attitude separately as in Figure 5. The outer loop is mainly responsible for tracking the desired angle of attack and generating the desired pitch angle velocity command, while the inner loop mainly tracks the desired pitch angle velocity to generate the elevator deflection command.

4.1.1. Attitude Outer Loop. The longitudinal rotational motion model of the aircraft is as follows:

$$\underbrace{\dot{\alpha}}_{\dot{x}_\alpha} = \underbrace{-(p\cos\alpha + r\sin\alpha)\tan\beta - \dot{\gamma}\frac{\cos\mu}{\cos\beta} - \dot{\chi}\frac{\sin\mu\cos\gamma}{\cos\beta}}_{f_\alpha} + q. \tag{30}$$

That is,

$$\dot{x}_\alpha = f_\alpha + q. \tag{31}$$

The attitude outer loop RBF-ADRC controller is as follows:

$$\begin{cases} \dot{v}_{\alpha 1} = v_{\alpha 2}, \\ \dot{v}_{\alpha 2} = \text{fhan}\,(v_{\alpha 1} - \alpha_d, v_{\alpha 2}, r, h), \\ \dot{z}_{01} = z_{12} - \beta_{01}(z_{01} - y_\alpha) + q, \\ \dot{z}_{02} = -\beta_{02}(z_{01} - y_\alpha), \\ e_1 = z_{01} - v_{\alpha 1}, \\ u_0 = \beta_1 fal(e_1, a_1, \delta), \\ q_d = u_0 - z_{02}. \end{cases} \tag{32}$$

The parameter β_1 is designed according to the above RBF-ADRC design method, and the gradient descent method is used to adjust β_1.

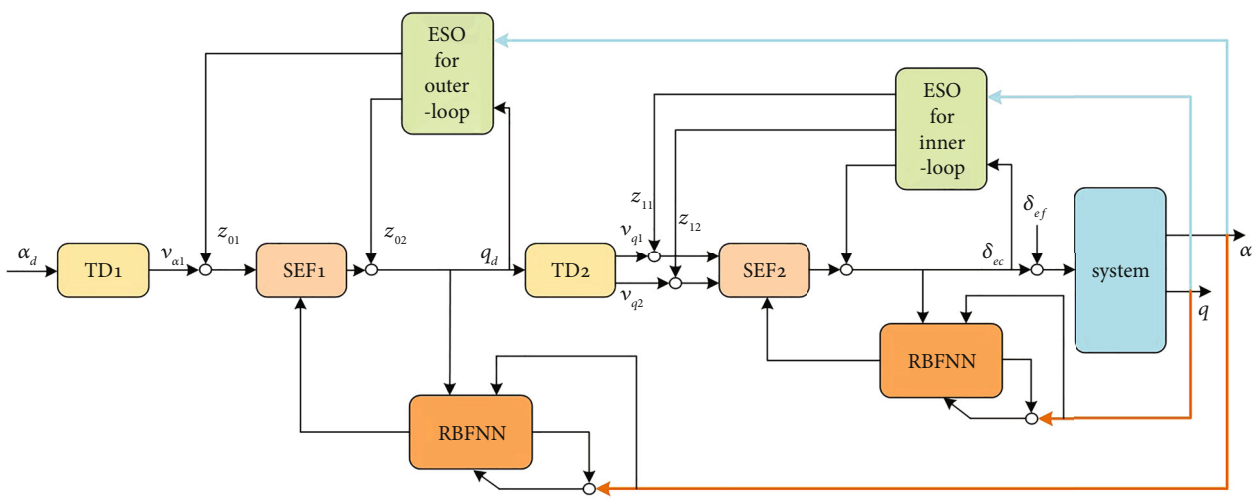

Figure 5: Diagram of attitude auxiliary channel based on cascaded RBF-ADRC.

4.1.2. Attitude Inner Loop. The equation for the longitudinal rotational dynamics is as follows:

$$\dot{q} = \frac{1}{I_{yy}}\left[M - (I_{xx} - I_{zz})pr - I_{xz}\left(p^2 - r^2\right)\right]. \tag{33}$$

The expression of pitching moment is as follows:

$$M = QS\bar{c}\left(C_{m_0} + C_{m_{\delta_e}}\delta_e + C_{m_{\delta_f}}\delta_f + \frac{\bar{c}}{2V}C_{m_q}q\right), \tag{34}$$

where $Q = (1/2)\rho U^2$ is the dynamic pressure, ρ is the density of air, S is the wing area, $\bar{c}$ is the aerodynamic mean chord, and C_{m_0}, $C_{m_{\delta_e}}$, C_{m_q}, and $C_{m_{\delta_f}}$ are aerodynamic coefficients.

$$\underbrace{\dot{q}}_{\dot{x}_1} = \underbrace{\frac{1}{I_{yy}}\left[QS\bar{c}\left(C_{m_0} + C_{m_{\delta f}}\delta_f + \frac{\bar{c}}{2V}C_{m_q}q\right) - (I_{xx} - I_{zz})pr - I_{xz}\left(p^2 - r^2\right)\right] + \frac{1}{I_{yy}}C_{m_{\delta_e}}QS\bar{c}\delta_{ef}}_{f_1} + \underbrace{\frac{1}{I_{yy}}C_{m_{\delta_e}}QS\bar{c}\,\delta_e}_{g_1}. \tag{35}$$

Since the elevator actuator is a first-order inertial link, the equation of the pitch angle velocity with respect to the elevator deflection becomes a second-order form

$$\ddot{x}_q = f_q + g_q\delta_{ec}. \tag{36}$$

The RBF-ADRC design for the attitude inner loop is as follows:

$$\begin{cases} \dot{v}_{q1} = v_{q2}, \\ \dot{v}_{q2} = \text{fhan}\left(v_{q1} - q_d, v_{q2}, r, h\right), \\ \dot{z}_{11} = z_{12} - \beta_{11}\left(z_{11} - y_q\right), \\ \dot{z}_{12} = z_{13} - \beta_{12}\left(z_{11} - y_q\right) + g_q\delta_{ec}, \\ \dot{z}_{13} = -\beta_{13}\left(z_{11} - y_q\right), \\ e_1 = z_{11} - v_{q1}, \\ e_2 = z_{12} - v_{q2}, \\ u_0 = \beta_1 fal(e_1, a_1, \delta) + \beta_2 \text{fal}(e_2, a_2, \delta), \\ \delta_{ec} = (u_0 - z_{13})g_q^{-1}. \end{cases} \tag{37}$$

The parameters β_1 and β_2 are designed according to the above RBF-ADRC design method, and the gradient descent method is used to adjust β_1 and β_2.

4.2. Approach Power Compensator System Controller Design Scheme. The APCS is used to automatically adjust the throttle to control the approach speed of the aircraft.

The dynamic for ground speed has the expression as

$$\dot{V} = \frac{(-D - mg\sin\gamma)}{m} + \frac{\cos\alpha\cos\beta}{m}P. \tag{38}$$

The engine thrust is expressed in equation (44).

$$P = (C_{\text{Ma}}\text{Ma} + C_h H)\delta_{pl}. \tag{39}$$

where C_{Ma} is the engine Mach number factor and C_h is the engine height factor.

$$\underbrace{\dot{V}}_{x_v} = \underbrace{\frac{(-D - mg\sin\gamma)}{m} + \frac{\cos\alpha\cos\beta}{m}(C_{\mathrm{Ma}}\mathrm{Ma} + C_h H)\delta_{pf}}_{f_v} + \underbrace{\frac{\cos\alpha\cos\beta}{m}(C_{\mathrm{Ma}}\mathrm{Ma} + C_h H)\delta_{pl}}_{g_v}. \tag{40}$$

The equation for the speed relative to the throttle lever deflection command is as follows:

$$\dot{x}_v = f_v + g_v\delta_{pl}. \tag{41}$$

The RBF-ADRC controller of APCS is as follows:

$$\begin{cases} \dot{v}_{v1} = v_{v2}, \\ \dot{v}_{v2} = \mathrm{fhan}(v_{v1} - V_d, v_{v2}, r, h), \\ \dot{z}_{21} = z_{22} - \beta_{21}(z_{21} - y_v) + g_v\delta_{pl}, \\ \dot{z}_{22} = -\beta_{22}(z_{21} - y_v), \\ e_1 = z_{21} - v_{v1}, \\ u_0 = \beta_1 \mathrm{fal}(e_1, a_1, \delta), \\ \delta_{pl} = (u_0 - z_{22})g_v^{-1}. \end{cases} \tag{42}$$

The parameter β_1 is designed according to the above RBF-ADRC design method, and the gradient descent method is used to adjust β_1.

4.3. Flight Path Control. Direct lift control was introduced into the trajectory control channel to provide lift directly to the shipboard aircraft through the flaps. Conventional automatic landings change the trajectory and altitude indirectly by changing the pitch angle, and the feedforward of the aircraft dynamics is $\delta_e \xrightarrow{\text{integration}} q \xrightarrow{\text{integration}} \theta/\alpha \xrightarrow{\text{integration}} \gamma \xrightarrow{\text{integration}} h$; the phase lag and the equivalent time delay are large. When DLC is used, the kinetic feedforward of the aircraft is $\delta_f \xrightarrow{\text{integration}} \gamma \xrightarrow{\text{integration}} h$, and the phase lag is greatly reduced.

4.3.1. The Longitudinal Guidance Law. The carrier-based aircraft was disturbed by air-wake during landing. Therefore, the longitudinal guidance law can be used to effectively suppress the interference.

The altitude deviation amount is calculated by the guidance law to get the trajectory angle command, which is transmitted to the flight control system. The lift force controls the trajectory angle directly and tracks the trajectory angle command quickly.

The guidance of the design uses the PID controller, and the control law is as follows:

$$\gamma_d = \left(K_p^H + K_i^H\frac{1}{s} + K_d^H s\right)(H_c - H) + \gamma_{\mathrm{ref}}. \tag{43}$$

The parameters in the control law can be obtained by debugging.

4.3.2. Direct Lift Channel. The dynamic equation describing the trajectory angle relative to the flight path is [38]

$$\dot{\gamma} = \frac{1}{-mU}[P(-\sin\alpha\cos\mu - \cos\alpha\sin\beta\sin\mu) + C\sin\mu - L\cos\mu + mg\cos\gamma]. \tag{44}$$

The expression for the lift force is

$$L = QS\left(C_{L_0} + C_{L_{\delta_e}}\delta_e + C_{L\alpha}\alpha + C_{L_{\delta_c}}\delta_c + C_{L_{\delta_f}}\delta_f\right), \tag{45}$$

where C_{L_0}, $C_{L_{\delta_e}}$, $C_{L\alpha}$, $C_{L_{\delta_c}}$, and $C_{L_{\delta_f}}$ are aerodynamic coefficients of the lift.

$$\underbrace{\dot{\gamma}}_{\dot{x}_2} = \underbrace{-\frac{1}{mV}\begin{bmatrix} P(-\sin\alpha\cos\mu - \cos\alpha\sin\beta\sin\mu) + C\sin\mu \\ -QS\left(C_{L_0} + C_{L_{\delta_e}}\delta_e + C_{L\alpha}\alpha + C_{L_{\delta_e}}\delta_c\right)\cos\mu + mg\cos\gamma \end{bmatrix} + \frac{QSC_{L_{\delta_f}}\cos\mu}{mV}\delta_{ff}}_{f_2} + \underbrace{\frac{QSC_{L_{\delta_f}}\cos\mu}{mV}}_{g_2}\delta_f. \tag{46}$$

Since the flap actuator is a first-order inertial link, the equation of the trajectory angle with respect to the flap deflection becomes a second-order form

$$\ddot{x}_\gamma = f_\gamma + g_\gamma\delta_{fc}. \tag{47}$$

The direct lift channel RBF-ADRC controller is as follows.

$$\begin{cases} \dot{v}_{\gamma 1} = v_{\gamma 2}, \\ \dot{v}_{\gamma 2} = \mathrm{fhan}\left(v_{\gamma 1} - \gamma_d, v_{\gamma 2}, R, h\right), \\ \dot{z}_{31} = z_{32} - \beta_{31}\left(z_{31} - y_\gamma\right), \\ \dot{z}_{32} = z_{33} - \beta_{32}\left(z_{31} - y_\gamma\right) + g_\gamma\delta_{fc}, \\ \dot{z}_{33} = -\beta_{33}\left(z_{31} - y_\gamma\right), \\ e_1 = z_{31} - v_{\gamma 1}, \\ e_2 = z_{32} - v_{\gamma 2}, \\ u_0 = \beta_1 fal(e_1, a_1, \delta) + \beta_2 fal(e_2, a_2, \delta), \\ \delta_{fc} = (u_0 - z_{33})g_\gamma^{-1}. \end{cases} \tag{48}$$

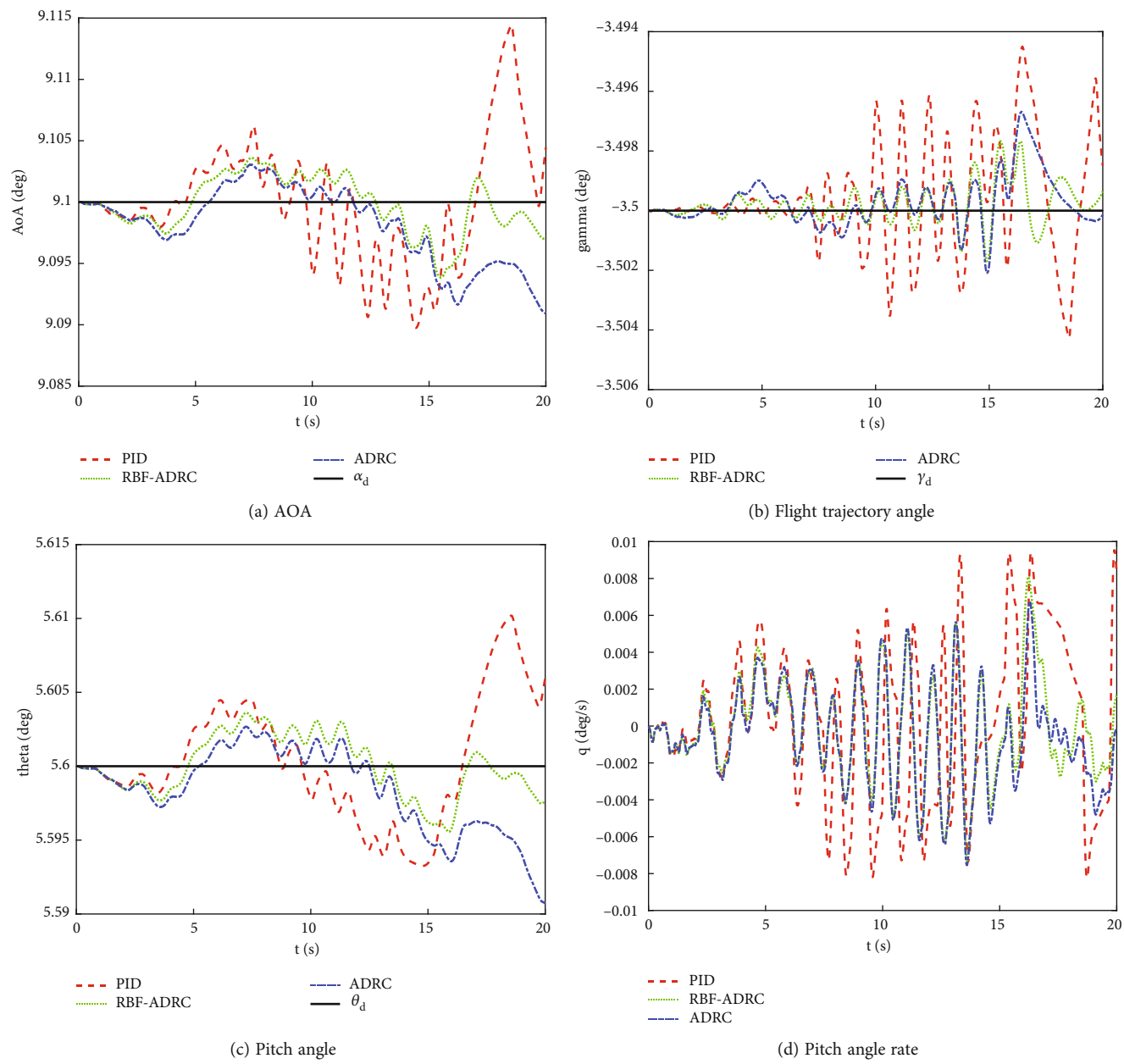

(a) AOA

(b) Flight trajectory angle

(c) Pitch angle

(d) Pitch angle rate

Figure 6: Comparison of aircraft attitude angle variation under the influence of constant faults.

The parameters β_1 and β_2 are designed according to the above RBF-ADRC design method, and the gradient descent method is used to adjust β_1 and β_2.

4.4. Stability Analysis of Closed-Loop Systems. The Lyapunov function is constructed as follows.

$$V(k) = \frac{1}{2}e_\alpha^2(k) + \frac{1}{2}e_\gamma^2(k) + \frac{1}{2}e_V^2(k) + \frac{1}{2}e_q^2(k). \tag{49}$$

$\Delta V(k)$ can be represented as

$$\begin{aligned}\Delta V(k) = {} & \frac{1}{2}e_\alpha^2(k)\eta_{\alpha x}\|\Gamma_{\alpha x}(k)\|^2\left[\eta_{\alpha x}\|\Gamma_{\alpha x}(k)\|^2 - 2\right] \\ & + \frac{1}{2}e_\gamma^2(k)\eta_{\gamma x}\|\Gamma_{\gamma x}(k)\|^2\left[\eta_{\gamma x}\|\Gamma_{\gamma x}(k)\|^2 - 2\right] \\ & + \frac{1}{2}e_V^2(k)\eta_{Vx}\|\Gamma_{Vx}(k)\|^2\left[\eta_{Vx}\|\Gamma_{Vx}(k)\|^2 - 2\right] \\ & + \frac{1}{2}e_q^2(k)\eta_{qx}\|\Gamma_{qx}(k)\|^2\left[\eta_{qx}\|\Gamma_{qx}(k)\|^2 - 2\right].\end{aligned} \tag{50}$$

If η_{ix} is chosen as

$$0 < \eta_{ix} < \frac{2}{\|\Gamma_{ix}(k)\|^2}\,(i = \alpha, \gamma, V, q), \tag{51}$$

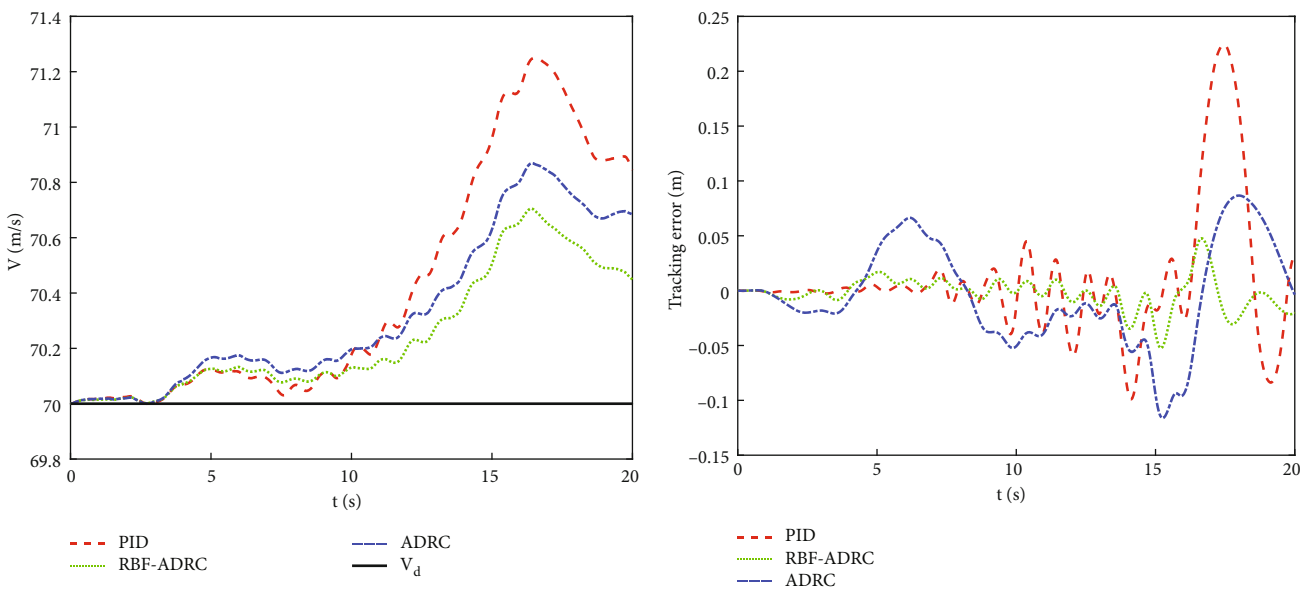

(a) Velocity error

(b) Tracking error

Figure 7: Trajectory track performance under the influence of constant faults.

then $\Delta V(k)$ in equation (50) will be less than zero. The Lyapunov stability of $V > 0$ and $\dot{V} < 0$ is guaranteed; therefore, the whole closed-loop system is stabilized.

5. Landing Simulation Results

When the carrier-based aircraft enters the entrance of the glide path, the initial condition is set as the flight altitude of the carrier-based aircraft is $h_0 = 114.3$ m, the reference height of the ideal landing point of the carrier-based aircraft is $h_c = 21.1$ m, and the reference velocity is $V_0 = 70$ m/s. The angle is controlled at $\alpha_0 = 9.1°$, and the reference glide path angle is controlled at $\gamma_{\text{ref}} = -3.5°$. In the simulation, RBF-ADRC is applied to DLC-ACLS to verify the automatic landing performance. In addition, the automatic landing performance of the RBF-ADRC scheme is compared with the traditional ADRC and the PID control scheme.

5.1. Constant Faults. Incorporating constant value failures in the actuators into the simulation experiments, the simulation results are shown in Figures 6 and 7 and the maximum deviation of variables is shown in Table 1. The engine fault $\delta_{pf} = 12°$ is introduced at $t = 4$ s. The elevator fault $\delta_{ef} = 8°$ is introduced at $t = 5$ s. The flap fault $\delta_{ff} = 8°$ is introduced at $t = 6$ s.

5.1.1. Stability Analysis. It can be seen from Figure 6(a) that when RBFNN is not introduced, the AOA angle deviation of traditional ADRC control is more significant. The AOA under the new design method is more stable through comparative analysis.

The deviation of the trajectory angle between the proposed method and the other two methods is compared in Figure 6(b), where "the proposed method" refers to the RBF-ADRC controller proposed in this paper. The comparative analysis shows that RBF-ADRC can better maintain the stability of the trajectory angle under the influence of faults and perturbations.

Table 1: The maximum deviation of variables at constant faults.

The error of variables	PID	ADRC	RBF-ADRC
Angle of attack error (deg)	0.0143	0.009	0.0061
Path angle error (deg)	0.0054	0.0032	0.0023
Pitch angle error (deg)	0.01	0.0092	0.0044
Pitch rate error (deg)	0.0094	0.0075	0.008
Velocity error (m/s)	1.25	0.87	0.7
Tracking error (m)	0.224	0.116	0.052

It can be seen from Figures 6(c) and 6(d) that after the introduction of RBFNN, compared with the traditional ADRC, the pitch angle deviation and pitch rate deviation fluctuations of the proposed method are significantly reduced, and the maximum deviation is reduced. In contrast, under the RBF-ADRC method, the flight attitude of the carrier-based aircraft can be better maintained. Reducing the deviation of flight attitude can make the carrier aircraft land more smoothly and enhance the robustness of the system.

5.1.2. Tracking Performance Analysis. From Figure 7(a), it can be seen that the velocity disturbance variation of the proposed method is significantly lower than that of PID. In contrast, the speed stability of the new design is better maintained, and the disturbance can be effectively suppressed. Figure 7(b) shows the trajectory tracking comparison of the proposed method and the other two methods. The height deviation represents the deviation between the simulated results and the ideal slope. It can be seen from

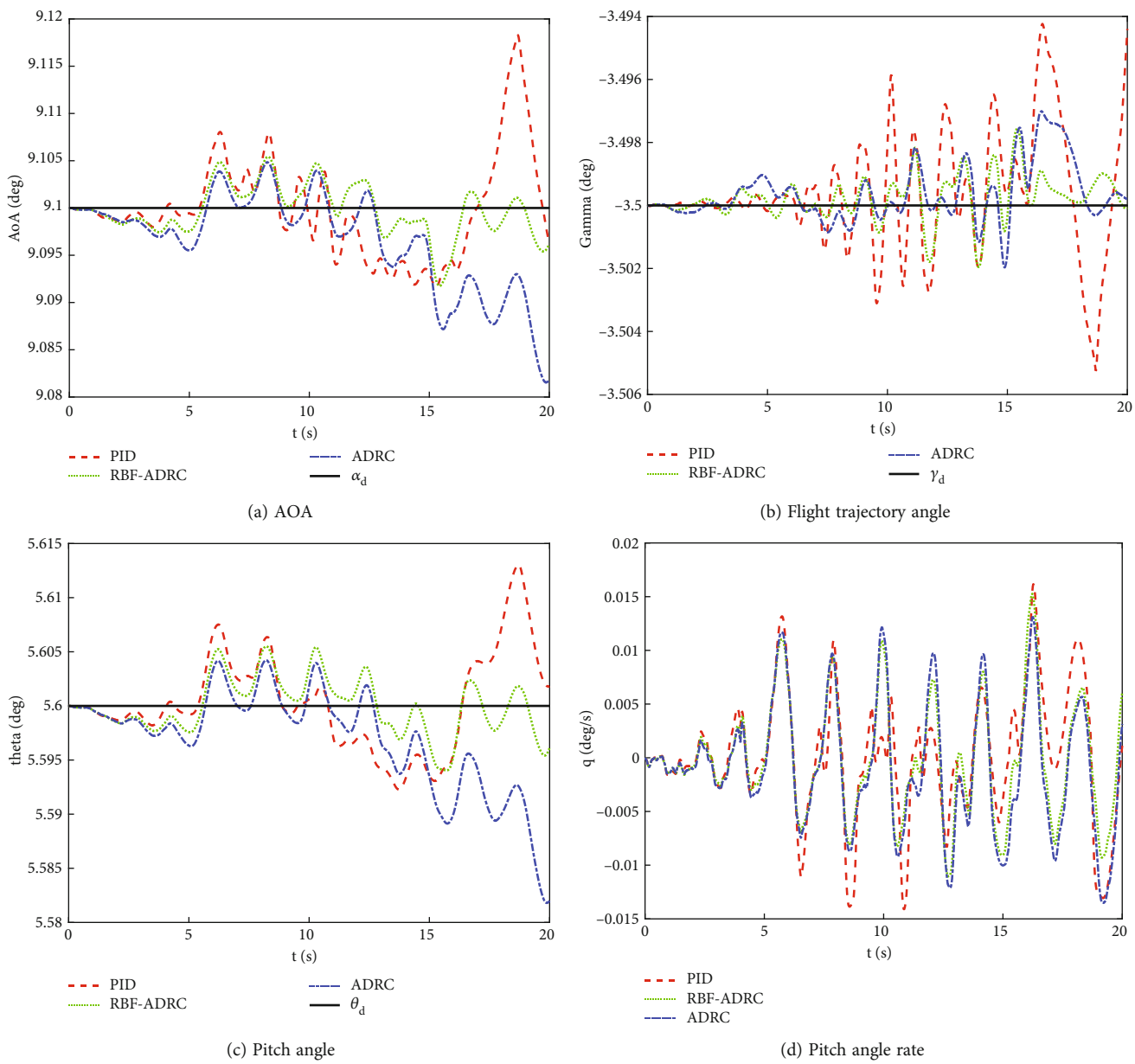

(a) AOA

(b) Flight trajectory angle

(c) Pitch angle

(d) Pitch angle rate

Figure 8: Comparison of aircraft attitude angle variation under the influence of time-varying faults.

Figure 7(b) that the tracking error of DLC-ACLS based on RBF-ADRC is within 0.113 m. The results show that the proposed DLC-ACLS based on RBF-ADRC can better track the ideal glide slope in the presence of faults and disturbances.

5.2. Time-Varying Faults. To enhance the assessment of the RBF-ADRC's robustness, the simulation experiment incorporates time-varying faults in the actuator; the simulation results are shown in Figure 8, and the maximum deviation of variables is shown in Table 2. The engine fault $\delta_{pf} = 12 \sin \pi t/2.5(^\circ)$ is introduced at $t = 4$ s. The elevator fault $\delta_{ef} = 8 \sin \pi t/2.5(^\circ)$ is introduced at $t = 5$ s. The flap fault $\delta_{ff} = 8 \sin \pi t/2.5(^\circ)$ is introduced at $t = 6$ s.

5.2.1. Stability Analysis. It can be seen from Figure 8(a) that when RBFNN is not introduced, the AOA angle deviation of traditional ADRC control is more significant. The AOA under the new design method is more stable through comparative analysis.

Table 2: The maximum deviation of variables during time-varying faults.

The error of variables	PID	ADRC	RBF-ADRC
Angle of attack error (deg)	0.018	0.018	0.00825
Path angle error (deg)	0.0057	0.0029	0.00239
Pitch angle error (deg)	0.129	0.018	0.006
Pitch rate error (deg)	0.0158	0.0134	0.015
Velocity error (m/s)	1.48	1.26	0.94
Tracking error (m)	0.278	0.125	0.051

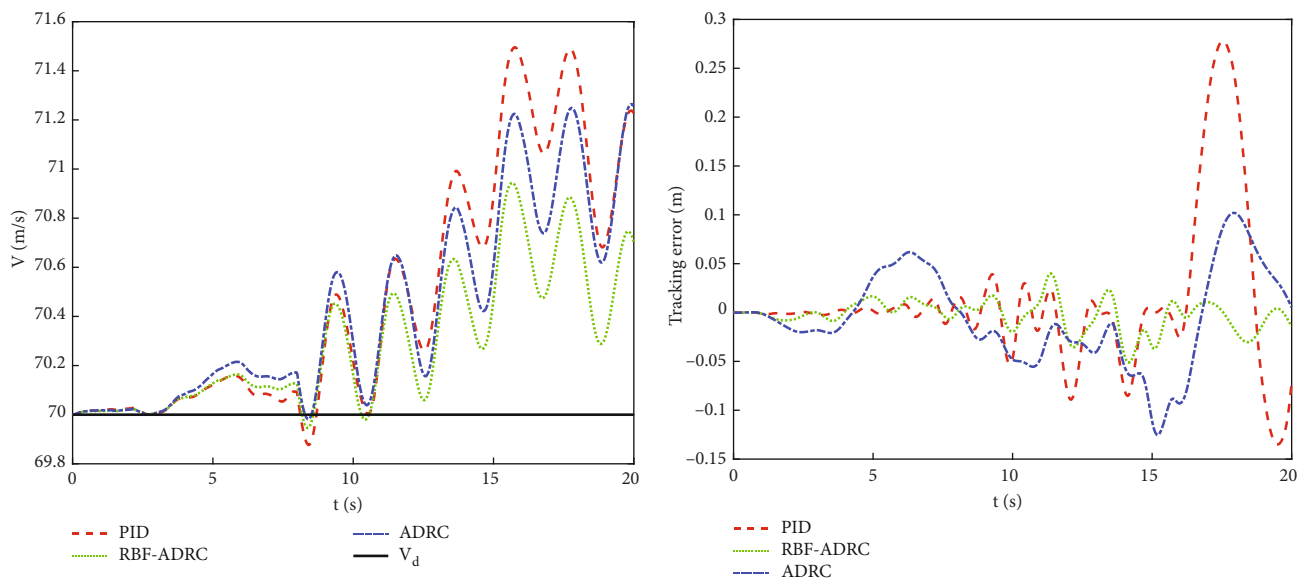

(a) Velocity error

(b) Tracking error

Figure 9: Trajectory track performance under the influence of time-varying faults.

5.2.2. Tracking Performance Analysis. As can be seen in Figure 9, the effect of time-varying faults on the aircraft speed is very large, and even with the newly designed method, the speed fluctuations remain large, but the fluctuations are relatively small compared to other methods. Figure 9 shows that the proposed method can track the error of the ideal glide path within a small range.

6. Summary

This paper introduces a novel robust fault-tolerant control strategy based on RBF-ADRC, designed and applied to a DLC-ACLS system suffering from wake disturbances and actuator failures. In this system, the attitude control channel precisely follows the desired angle of attack, the APCS automatically adjusts the throttle to control the aircraft's approach speed, and the direct lift control channel tracks the desired trajectory angle command. This study considers actuator failures and air-wake disturbances as total disturbances, estimated and compensated by ADRC. The parameters of ADRC are designed in real time using RBFNN.

To verify the effectiveness of the RBF-ADRC scheme, actuator constant faults and time-varying faults are introduced. Comparing the proposed control scheme with PID controller and traditional ADRC, the results show that the proposed method can not only quickly and effectively compensate for actuator faults and enhance fault tolerance but also significantly improve the robustness of the system. Further research will be conducted to investigate how to utilize the robustness and learning capability of the method to deal with complex control problems such as saturation of control inputs of the landing system.

Data Availability

The data that support the findings of this study are available on request from the corresponding author, upon reasonable request and with permission of laboratory confidentiality agency permission.

Conflicts of Interest

The authors declared that they have no conflicts of interest regarding this work.

Acknowledgments

This research was funded by the National Natural Science Foundation of China (Grant Number 52171299).

References

[1] Z. Zhen, S. Jiang, and J. Jiang, "Preview control and particle filtering for automatic carrier landing," *IEEE Transactions on Aerospace and Electronic Systems*, vol. 54, no. 6, pp. 2662–2674, 2018.

[2] H. Duan, Y. Yang, and Z. Zeng, "Automatic carrier landing system with fixed time control," *IEEE Transactions on Aerospace and Electronic Systems*, vol. 58, no. 4, pp. 3586–3600, 2022.

[3] Z. Zheng, Z. Jin, L. Sun, and M. Zhu, "Adaptive sliding mode relative motion control for autonomous carrier landing of fixed-wing unmanned aerial vehicles," *IEEE Access*, vol. 5, pp. 5556–5565, 2017.

[4] M. Lungu, "Auto-landing of fixed wing unmanned aerial vehicles using the backstepping control," *ISA Transactions*, vol. 95, pp. 194–210, 2019.

[5] A. K. Bhatia, J. Jiang, A. Kumar, S. A. A. Shah, A. Rohra, and Z. ZiYang, "Adaptive preview control with deck motion compensation for autonomous carrier landing of an aircraft," *International Journal of Adaptive Control and Signal Processing*, vol. 35, no. 5, pp. 769–785, 2021.

[6] Z. Guan, H. Liu, Z. Zheng, M. Lungu, and Y. Ma, "Fixed-time control for automatic carrier landing with disturbance," *Aerospace Science and Technology*, vol. 108, article 106403, 2021.

[7] M. Lungu, D.-A. Dinu (Vîlcică), M. Chen, and G. Flores, "Inverse optimal control for autonomous carrier landing with disturbances," *Aerospace Science and Technology*, vol. 139, article 108382, 2023.

[8] Q. Zhu and Z. Yang, "Design of air-wake rejection control for longitudinal automatic carrier landing cyber-physical system," *Computers & Electrical Engineering*, vol. 84, article 106637, 2020.

[9] F. Luo, J. Zhang, P. Lyu, Z. Liu, and W. Tang, "Carrier-based aircraft precision landing using direct lift control based on incremental nonlinear dynamic inversion," *IEEE Access*, vol. 10, pp. 55709–55725, 2022.

[10] M. DeSalvo, D. Heathcote, M. J. Smith, and A. Glezer, "Direct lift control using distributed aerodynamic bleed," in *AIAA Scitech 2019 Forum*, p. 0591, San Diego, California, January 2019.

[11] S. Ijaz, L. Yan, M. T. Hamayun, and C. Shi, "Active fault tolerant control scheme for aircraft with dissimilar redundant actuation system subject to hydraulic failure," *Journal of the Franklin Institute*, vol. 356, no. 3, pp. 1302–1332, 2019.

[12] L. Chen, C. Edwards, H. Alwi, and M. Sato, "Flight evaluation of a sliding mode online control allocation scheme for fault tolerant control," *Automatica*, vol. 114, article 108829, 2020.

[13] H. Gao, W. He, Y. Zhang, and C. Sun, "Adaptive finite-time fault-tolerant control for uncertain flexible flapping wings based on rigid finite element method," *IEEE Transactions on Cybernetics*, vol. 52, no. 9, pp. 9036–9047, 2022.

[14] F. Nan, S. Sun, P. Foehn, and D. Scaramuzza, "Nonlinear MPC for quadrotor fault-tolerant control," *IEEE Robotics and Automation Letters*, vol. 7, no. 2, pp. 5047–5054, 2022.

[15] X. Wang and E.-J. Van Kampen, "Incremental backstepping sliding mode fault-tolerant flight control," in *AIAA Scitech 2019 Forum*, San Diego, California, January 2019.

[16] H. An, J. Liu, C. Wang, and L. Wu, "Approximate backstepping fault-tolerant control of the flexible air-breathing hypersonic vehicle," *IEEE/ASME Transactions on Mechatronics*, vol. 21, no. 3, pp. 1680–1691, 2015.

[17] Y. Zhang, J. Liu, and W. He, "Adaptive fault-tolerant control for a nonlinear flexible aircraft wing system," *Asian Journal of Control*, vol. 21, no. 5, pp. 2340–2351, 2019.

[18] S. Zhang and Q. Meng, "An anti-windup INDI fault-tolerant control scheme for flying wing aircraft with actuator faults," *ISA Transactions*, vol. 93, pp. 172–179, 2019.

[19] J. Li and H. Duan, "Simplified brain storm optimization approach to control parameter optimization in F/A-18 automatic carrier landing system," *Aerospace Science and Technology*, vol. 42, pp. 187–195, 2015.

[20] R. Dou and H. Duan, "Lévy flight based pigeon-inspired optimization for control parameters optimization in automatic carrier landing system," *Aerospace Science and Technology*, vol. 61, pp. 11–20, 2017.

[21] H. Duan, L. Chen, and Z. Zeng, "Automatic landing for carrier-based aircraft under the conditions of deck motion and carrier airwake disturbances," *IEEE Transactions on Aerospace and Electronic Systems*, vol. 58, no. 6, pp. 5276–5291, 2022.

[22] M. Lungu, M. Chen, and D.-A. Vîlcică (Dinu), "Backstepping- and sliding mode-based automatic carrier landing system with deck motion estimation and compensation," *Aerospace*, vol. 9, no. 11, p. 644, 2022.

[23] M. A. Lotufo, L. Colangelo, C. Perez-Montenegro, E. Canuto, and C. Novara, "UAV quadrotor attitude control: An ADRC-EMC combined approach," *Control Engineering Practice*, vol. 84, pp. 13–22, 2019.

[24] J. Liu, M. Sun, Z. Chen, and Q. Sun, "High AOA decoupling control for aircraft based on ADRC," *Journal of Systems Engineering and Electronics*, vol. 31, no. 2, pp. 393–402, 2020.

[25] F. Doostdar and H. Mojallali, "An ADRC-based backstepping control design for a class of fractional-order systems," *ISA Transactions*, vol. 121, pp. 140–146, 2022.

[26] S. Yu, L. Liu, L. Han, and X. Sun, "Research on ultra-high power laser curing based on RBF neural network," in *2022 Global Conference on Robotics, Artificial Intelligence and Information Technology (GCRAIT)*, pp. 290–293, Chicago, IL, USA, July 2022.

[27] H. Yang and J. Liu, "An adaptive RBF neural network control method for a class of nonlinear systems," *IEEE/CAA Journal of Automatica Sinica*, vol. 5, no. 2, pp. 457–462, 2018.

[28] H.-G. Han, W. Lu, Y. Hou, and J.-F. Qiao, "An adaptive-PSO-based self-organizing RBF neural network," *IEEE Transactions on Neural Networks and Learning Systems*, vol. 29, no. 1, pp. 104–117, 2018.

[29] Q. Wu, Q. Zhu, and S. Han, "Elman neural network-based direct lift automatic carrier landing nonsingular terminal sliding mode fault-tolerant control system design," *Computational Intelligence and Neuroscience*, vol. 2023, Article ID 3560441, 15 pages, 2023.

[30] J. W. Denham, "Project MAGIC CARPET: "advanced controls and displays for precision carrier landings"," in *54th AIAA Aerospace Sciences Meeting*, p. 1770, San Diego, California, USA, January 2016.

[31] Z. Wen, Z. Zhi, Z. Qidan, and X. Shiyue, "Dynamics model of carrier-based aircraft landing gears landed on dynamic deck," *Chinese Journal of Aeronautics*, vol. 22, no. 4, pp. 371–379, 2009.

[32] Z. Lan, "Applications of BP, convolutional and RBF networks," in *2021 2nd International Conference on Computing and Data Science (CDS)*, pp. 543–547, Stanford, CA, USA, January 2021.

[33] F. Yang, C. Guo, and Y. Jiang, "RBF based integrated ADRC controller for a ship dynamic positioning system," in *Proceedings of 2017 Chinese Intelligent Automation Conference*pp. 673–680, Springer, Singapore.

[34] J. Han and W. Wang, "Nonlinear tracking-differentiator," *Journal of Systems Science and Mathematical Sciences*, vol. 14, no. 2, p. 177, 1994.

[35] Y. Zhang, Z. Chen, X. Zhang, Q. Sun, and M. Sun, "A novel control scheme for quadrotor UAV based upon active disturbance rejection control," *Aerospace Science and Technology*, vol. 79, pp. 601–609, 2018.

[36] J. Han, "From PID to active disturbance rejection control," *IEEE Transactions on Industrial Electronics*, vol. 56, no. 3, pp. 900–906, 2009.

[37] Z. Gao, "Scaling and bandwidth-parameterization based controller tuning," in *Proceedings of the 2003 American Control Conference, 2003*, pp. 4989–4996, Denver, CO, USA, June 2003.

[38] Z. Guan, Y. Ma, Z. Zheng, and N. Guo, "Prescribed performance control for automatic carrier landing with disturbance," *Nonlinear Dynamics*, vol. 94, no. 2, pp. 1335–1349, 2018.